DEPENDENCE OF STEP SIZE IN THE CONTINUUM STRONG DISCONTINUITY APPROACH USING THE BOUNDARY ELEMENT METHOD

T.S. Mendonça

R.G. Peixoto

G.O. Ribeiro

tiagodesouzamendonca@gmail.com

rodrigo.peixoto@dees.ufmg.br

gabriel@dees.ufmg.br

Universidade Federal de Minas Gerais, Departamento de Engenharia de Estruturas

Av. Antônio Carlos 6627, 31270-901, Minas Gerais, Belo Horizonte, Brazil

Abstract. *The failure analysis in structures is extremely important since it allows to evaluate the safety degree and the integrity of structural systems. However, despite the increasing use of numerical methods in the study of material failures in the last years, the boundary element method is still little used when compared to domain methods. Thus, in this work it is analyzed the failure mechanics in some classical problems through the continuum strong discontinuity approach. In this way, it is used the implicit formulation of the boundary element method for nonlinear problems to shown the dependence of the step size when the cells with embedded discontinuity are generated only after step convergence or during any iteration, respectively, in the incremental-iterative process. For this purpose, the same problem was analyzed considering these two cases and also different numbers of steps. It was verified that the results are coincident for all numbers of steps considered in the simulations when cells are generated during any iteration, showing step size independence in this case, while the same is not true for the case of cells generated only after convergence, in which a large numbers of steps is required for well accuracy.*

Keywords: *Implicit boundary element method, Continuum strong discontinuity approach, Failure mechanics, Step size dependence*

1 INTRODUCTION

The increasing progress in the development of computational resources in recent years has led to an increase in the use of numerical methods in engineering. In this sense, the numerical study of material failures has been one of the most prominent areas, since analytical solutions are scarce and experimental tests are usually expensive and laborious. Moreover, this type of study is of great importance in the design of several types of structures, since it allows a determination of the post-critical behavior when such structures are subject to overload, thus contributing to the establishment of techniques to predict structural collapse. However, in spite of the extensive use of domain numerical methods in the analysis of material failures, such as the finite element method, the boundary element method is still little used even though it has the advantage of discretization only the boundary domain.

Numerical techniques for simulation of material failures have been developed and among these, one that has stood out is the continuum strong discontinuity approach initially introduced by Simo et al. (1993). In this technique, it is considered a kinematics characterized by the presence of finite discontinuities in the displacement field and, consequently, infinite discontinuities in the strain field. In this way, it is shown that continuous constitutive models, equipped with a strain softening law, are compatible with the kinematics of strong discontinuities and thus induce a discrete constitutive model on the discontinuous surface (Oliver, 2000; Oliver et al., 2002). Later on, in Oliver (1996a) and Oliver (1996b), a more rigorous detailing of the process of identifying the characteristics that make conventional continuous constitutive models consistent with the strong discontinuity regime was carried out. In addition, a more general numerical treatment with the finite element method, using isotropic damage models and elastoplastic models, to show that the analysis methodology is easily extended to any constitutive model was considered.

In many cases, the kinematics of strong discontinuity can be induced directly after the elastic regime. However, in some cases, it becomes necessary to consider an intermediate phase when the so-called strong discontinuity conditions are not met at the moment of bifurcation which is characterized by a formation of a strain localization zone. These conditions consist of a set of equations necessary for the compatibilization of the continuous constitutive model to the strong discontinuity regime. In this case, a transitional phase between the bifurcation and the strong discontinuity based on weak discontinuity kinematics is considered in the works of Manzoli et al. (1998), Oliver et al. (1998), Oliver et al. (1999) and Peixoto et al. (2016). This kinematics is characterized by continuous displacements fields and the presence of finite discontinuities in the strain field. In addition, these works also take into account a regularized kinematics capable of representing both (weak and strong) kinematics through a single set of equations. In this way, a variable band model is presented where the localization band thickness, represented by a scalar factor of finite initial value, decreases until, at the limit, when this value tends to zero, the strong discontinuity kinematics is obtained. Therefore, it is shown that this model is more suitable to represent the regions of the fracture process zone.

The works presented so far has used the finite element method to demonstrate the effectiveness of the continuum strong discontinuity approach. However, the boundary element method was also employed, although it still has very limited use. In this sense, the works of Manzoli and Venturini (2004) and Manzoli and Venturini (2007) consider constant cells with embedded discontinuity and use associative elastoplastic constitutive models with a specific flow criterion,

together with an exponential softening law, to represent the behavior of fractures in quasi-brittle materials. In Pedrini (2008) and Manzoli et al. (2009) the same idea of these works is used, however, using an isotropic damage model. In all these studies only two-dimensional problems and triangular cells were considered. In addition, the strong discontinuity was imposed directly after the end of the elastic regime with the direction of the discontinuity line defined as perpendicular to the maximum principal stress.

In this article a material failure analysis is performed through the implicit formulation of the boundary element method using the continuum strong discontinuity approach that was implemented in the INSANE software (INteractive Structural ANalysis Environment) through the work of Peixoto et al. (2017). Thus, considering a classical problem in the literature with monotonic load, the strong discontinuity regime is introduced directly after the end of the elastic regime with the direction of the discontinuity line perpendicular to the maximum principal stress. Besides this, using an automatic cell generation algorithm, the analyzes are performed considering generation of cells with embedded discontinuity in any iteration and also only after step convergence that, from the numerical point of view, would be the most correct because it refers to a equilibrium situation. Therefore, in the first case, step size independence with satisfactory results is observed while, in the latter case, a large numbers of steps is required for well accuracy.

2 ISOTROPIC DAMAGE CONSTITUTIVE MODEL

2.1 Constitutive equations

In the numerical analyzes performed in this work, a isotropic damage constitutive model is used. This model can be synthesized through the following equations (Peixoto et al., 2017):

$$\psi(\epsilon_{ij}, r) = [1 - D(r)]\psi_o(\epsilon_{ij}), \quad \psi_o(\epsilon_{ij}) = \frac{1}{2}\epsilon_{ij} E^o_{ijkl} \epsilon_{kl} \tag{1}$$

$$\sigma_{ij} = \frac{\partial \psi(\epsilon_{ij}, r)}{\partial \epsilon_{ij}} = (1 - D) E^o_{ijkl} \epsilon_{kl} = E_{ijkl} \epsilon_{kl} \tag{2}$$

$$D \equiv D(r) = 1 - \frac{q(r)}{r}, \quad D \in [0, 1] \tag{3}$$

$$\dot{r} = \dot{\gamma}, \quad \begin{cases} r \in [r_o, \infty), \\ r_o = r|_{t=0} = \frac{f_t}{\sqrt{E}} \end{cases} \tag{4}$$

$$\bar{F}(\epsilon_{ij}, r) = \tau_\epsilon - r \tag{5}$$

$$\bar{F} \leqslant 0, \quad \dot{\gamma} \geqslant 0, \quad \dot{\gamma}\bar{F} = 0, \quad \dot{\gamma}\dot{\bar{F}} = 0 \tag{6}$$

$$\dot{q} = H(r)\dot{r}, \quad (H = q'(r) \leqslant 0), \quad \begin{cases} q \in [0, r_o], \\ q|_{t=0} = r_o \end{cases} \tag{7}$$

The Eq. (1) represents the expression for Helmholtz free energy. In this equation the term r is the strain-like scalar internal variable. In addition, D is the damage variable and E^o_{ijkl} represents the elastic constitutive tensor for isotropic materials which is given by:

$$E^o_{ijkl} = \bar{\lambda}\delta_{ij}\delta_{kl} + \mu(\delta_{ik}\delta_{jl} + \delta_{il}\delta_{jk}) \tag{8}$$

where δ_{ij} is the Kronecker delta and the terms μ and $\bar{\lambda}$ represent the Lamé constants that are expressed as:

$$\mu = \frac{E}{2(1+\nu)}; \quad \bar{\lambda} = \frac{2\mu\bar{\nu}}{1-2\bar{\nu}} \tag{9}$$

where E is the elasticity modulus, ν is the Poisson's ratio and $\bar{\nu}$ is given by:

$$\bar{\nu} = \begin{cases} \nu, & \text{for 3D and plane strain state} \\ \dfrac{\nu}{1+\nu}, & \text{for plane stress state} \end{cases} \tag{10}$$

Already the Eqs. (2), (3), (4), (5) and (7) represent, respectively, a constitutive equation, an expression for the damage variable, the evolution law of the internal variable, a damage criterion, and a softening law. In these expressions, the term σ_{ij} represents the Cauchy stress tensor, E_{ijkl} represents the secant tensor of the constitutive relation, q is the stress-like internal scalar variable, γ is the damage multiplier, f_t refers to the tensile strength, $\bar{F}$ represents the damage function in the strain space, τ_ϵ is the equivalent strain and H is the hardening-softening modulus. And finally, the Eq. (6) expresses consistency and Kuhn-Tucker conditions.

Different damage criteria can be obtained from the choice of the τ_ϵ parameter (Eq. (5)). In this work, the damage criterion proposed by Oliver et al. (2006) is adopted, that is:

$$\tau_\epsilon = \sqrt{\epsilon_{ij}^{+} E_{ijkl}^{o} \epsilon_{kl}} \tag{11}$$

In the Eq. (11) the tensor ϵ_{ij}^{+} is defined, taking into account a coordinate system aligned with the strain principal directions, such as:

$$\epsilon_{ij}^{+} = \sum_{k=1}^{n_{dim}} \langle \epsilon_k \rangle \hat{\mathbf{e}}_k \otimes \hat{\mathbf{e}}_k \tag{12}$$

In the Eq. (12) the term ϵ_k represents the *k*-th principal strain, $\hat{\mathbf{e}}_k$ represents a unit vector in the corresponding principal direction and $\langle \epsilon_k \rangle = (|\epsilon_k| + \epsilon_k)/2$. Thus, this model becomes suitable in the representation of quasi-brittle materials, since the degradation will occur in traction states preferentially.

And finally, an incremental constitutive equation can be obtained from the Eq. (2) considering the inelastic loading condition ($\dot{r} = \dot{\tau}_\epsilon$), that is:

$$\begin{aligned} \dot{\sigma}_{ij} &= (1-D) E_{ijkl}^{o} \dot{\epsilon}_{kl} - \dot{D} E_{ijkl}^{o} \epsilon_{kl} \\ &= E_{ijkl} \dot{\epsilon}_{kl} - \left(\frac{\partial D}{\partial r} \right) \dot{r} E_{ijkl}^{o} \epsilon_{kl} \\ &= \left[E_{ijkl} - \left(\frac{\partial D}{\partial r} \right) \left(\frac{\partial \tau_\epsilon}{\partial \epsilon_{kl}} \right) E_{ijrs}^{o} \epsilon_{rs} \right] \dot{\epsilon}_{kl} \\ &= E_{ijkl}^{t} \dot{\epsilon}_{kl} \end{aligned} \tag{13}$$

where E_{ijkl}^{t} is the constitutive tangent tensor.

2.2 Softening law

For the strong discontinuity regime an exponential softening law is adopted for the Eq. (7), that is:

$$q(r) = r_o e^{\frac{r_o^2 k}{G_f}\left(1-\frac{r}{r_o}\right)} \tag{14}$$

where G_f represents the fracture energy and k is the band thickness that, for the strong discontinuity regime, is approximately equal to zero $(k \approx 0)$. Moreover, in obtaining this equation, the direct introduction of the strong discontinuity regime after the end of the elastic regime was considered.

From Eqs. (3) and (14) we find the following expression for the damage variable (Peixoto et al., 2017):

$$D(r) = 1 - \frac{r_o}{r} e^{\frac{r_o^2 k}{G_f}\left(1-\frac{r}{r_o}\right)} \quad \text{for} \quad r > r_o \tag{15}$$

3 INTEGRAL EQUATIONS FOR PHYSICALLY NONLINEAR PROBLEMS

3.1 Strong discontinuity kinematics

A strong discontinuity kinematics capable of to distribute the effects of the discontinuous surface on a finite region of the domain is presented. Thus, with reference to Fig. 1, a subdomain Ω_φ is defined initially around a discontinuity line $\mathcal{S}$ and contained in the domain Ω.

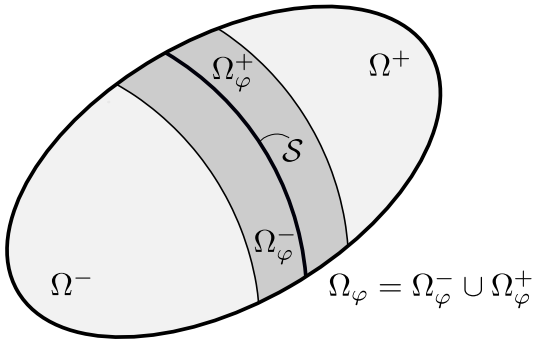

Figure 1: Discontinuous surface contained in an arbitrary subdomain Ω_φ

Also is defined a continuous and arbitrary function in $\Omega_\varphi(\mathbf{X})$, such that $\varphi(\mathbf{X}) = 0$ in $\Omega^- \backslash \Omega_\varphi^-$ and $\varphi(\mathbf{X}) = 1$ in $\Omega^+ \backslash \Omega_\varphi^+$. In these case, the expression $a \backslash b$ means the domain a excluding the domain b, that is, $a \backslash b = a - (a \cap b)$ and, besides this, the material points are designated by $\mathbf{X}$. Thus, can be defined the following equation:

$$\begin{aligned} \dot{u}_i(\mathbf{X},t) &= \underbrace{\dot{\bar{u}}_i(\mathbf{X},t) + \varphi(\mathbf{X})[\![\dot{u}_i]\!](\mathbf{X},t)}_{\dot{\hat{u}}_i(\mathbf{X},t)} + \underbrace{[\mathcal{H}_{\mathcal{S}}(\mathbf{X}) - \varphi(\mathbf{X})]}_{\mathcal{M}_{\mathcal{S}}^{\varphi}(\mathbf{X})}[\![\dot{u}_i]\!](\mathbf{X},t) \\ &= \dot{\hat{u}}_i(\mathbf{X},t) + \mathcal{M}_{\mathcal{S}}^{\varphi}(\mathbf{X})[\![\dot{u}_i]\!](\mathbf{X},t) \end{aligned} \tag{16}$$

where the terms $\dot{u}_i(\mathbf{X},t)$, $[\![u_i]\!](\mathbf{X},t)$ and $\mathcal{H}_\mathcal{S}(\mathbf{X})$ represent, respectively, the components of the regular part of the displacement field, the components of displacement jumps on the discontinuity surface $\mathcal{S}$ and the Heaviside function ($\mathcal{H}_\mathcal{S}=1$ for $\mathbf{X}\in\Omega^+$ and $\mathcal{H}_\mathcal{S}=0$ for $\mathbf{X}\in\Omega^-$). In additon, $\hat{\dot{u}}_i(\mathbf{X},t)$ are continuous functions and $\mathcal{M}^\varphi_\mathcal{S}(\mathbf{X})$ has null value for all $\mathbf{X}$ in Ω, except for $\mathbf{X}\in\Omega_\varphi$.

Therefore, with the kinematic defined by the Eq. (16) the essential boundary conditions (prescribed displacements) can be applied exclusively to the terms $\hat{u}_i$, since $\Gamma_u \cap \Omega_\varphi = 0$. In this case Γ_u represents the region of the boundary where the essential boundary conditions are applied.

The strains are given by the gradient of the symmetric part of the Eq. (16), that is:

$$\begin{aligned}\dot{\epsilon}_{ij}(\mathbf{X},t) &= \underbrace{\frac{1}{2}(\hat{\dot{u}}_{i,j}+\hat{\dot{u}}_{j,i})}_{\hat{\dot{\epsilon}}_{ij}} + \underbrace{\frac{\mathcal{M}^\varphi_\mathcal{S}}{2}([\![\dot{u}_{i,j}]\!]+[\![\dot{u}_{j,i}]\!]) - \frac{1}{2}(\varphi_{,i}[\![\dot{u}_j]\!]+\varphi_{,j}[\![\dot{u}_i]\!])}_{-\dot{\epsilon}^\varphi_{ij}} \\ &\qquad + \frac{\delta_\mathcal{S}}{2}([\![\dot{u}_i]\!]n_j+[\![\dot{u}_j]\!]n_i) \\ &= \hat{\dot{\epsilon}}_{ij} - \dot{\epsilon}^\varphi_{ij} + \frac{\delta_\mathcal{S}}{2}([\![\dot{u}_i]\!]n_j+[\![\dot{u}_j]\!]n_i)\end{aligned} \tag{17}$$

where the term $\hat{\epsilon}_{ij}$ represents a regular portion of the strain field and the term ϵ^φ_{ij} has non-zero values only in Ω_φ.

3.2 Integral equations with discontinuities

The boundary value problem for a solid medium with the presence of a discontinuity surface $\mathcal{S}$ is represented by the following equations:

$$\dot{\sigma}_{ij,j}+\dot{b}_i = 0 \quad \text{for} \quad \mathbf{X}\in\Omega\backslash\mathcal{S} \tag{18}$$
$$\dot{\sigma}^+_{ij}n_j - \dot{\sigma}^-_{ij}n_j = 0 \quad \text{for} \quad \mathbf{X}\in\mathcal{S} \tag{19}$$
$$\dot{\sigma}^+_{ij}n_j - \dot{\sigma}^\mathcal{S}_{ij}n_j = \dot{\sigma}^-_{ij}n_j - \dot{\sigma}^\mathcal{S}_{ij}n_j = 0 \quad \text{for} \quad \mathbf{X}\in\mathcal{S} \tag{20}$$
$$\dot{\epsilon}_{ij} - \frac{1}{2}(\dot{u}_{i,j}+\dot{u}_{j,i}) = 0 \quad \text{for} \quad \mathbf{X}\in\Omega \tag{21}$$
$$\dot{\sigma}_{ij} = \dot{\sigma}^\mathcal{S}_{ij}(\dot{\epsilon}_{ij}) \quad \text{for} \quad \mathbf{X}\in\mathcal{S} \tag{22}$$
$$\dot{\sigma}_{ij} = \dot{\sigma}^{\Omega\backslash\mathcal{S}}_{ij}(\dot{\epsilon}_{ij}) = E^o_{ijkl}\dot{\epsilon}_{kl} \quad \text{for} \quad \mathbf{X}\in\Omega\backslash\mathcal{S} \tag{23}$$
$$\hat{\dot{u}}_i = \dot{\mathbb{u}}_i \quad \text{for} \quad \mathbf{X}\in\Gamma_u \tag{24}$$
$$\dot{\sigma}_{ij}n_j = \dot{\mathbb{t}}_i \quad \text{for} \quad \mathbf{X}\in\Gamma_\sigma \tag{25}$$

Equations (18), (19), (20), (21), (22), (23), (24) and (25) represent internal equilibrium, external continuity of surface forces, internal continuity of surface forces, kinematic compatibility, the constitutive compatibility in $\mathcal{S}$, the constitutive compatibility in $\Omega\backslash\mathcal{S}$, the essential boundary conditions and the natural boundary conditions, respectively. In these expressions, the terms $\dot{b}_i$, $\dot{\sigma}^+_{ij}$, $\dot{\sigma}^-_{ij}$, $\dot{\sigma}^\mathcal{S}_{ij}$, $\dot{\sigma}^\mathcal{S}_{ij}(\dot{\epsilon}_{ij})$, $\dot{\mathbb{u}}_i$ and $\dot{\mathbb{t}}_i$ represent the rates of the body forces, of the stresses in Ω^+, of the stresses in Ω^-, of the stresses in $\mathcal{S}$, of an appropriate continuous constitutive relation, of the prescribed displacements and of the prescribed surface forces, respectively. In addition,

in the Eq. (24), as mentioned previously, Γ_u is the boundary region where the displacements are prescribed and Γ_σ, in the Eq. (25), is the boundary region where surface forces are prescribed. It should also be noted, through the Eq. (23), that a linear elastic regime is considered for $\Omega\backslash\mathcal{S}$.

The constitutive relations present in the Eqs. (22) and (23) can be rewritten, after applying the Eq. (17), as follows:

$$\dot{\sigma}_{ij}^{\mathcal{S}}(\dot{\epsilon}_{ij}) = \dot{\sigma}_{ij}^{\mathcal{S}}(\dot{\hat{\epsilon}}_{ij}, [\![\dot{u}_i]\!], [\![\dot{u}_{i,j}]\!]) \tag{26}$$

$$\dot{\sigma}_{ij}^{\Omega\backslash\mathcal{S}}(\dot{\epsilon}_{ij}) = E_{ijkl}^{o}\dot{\epsilon}_{kl} = E_{ijkl}^{o}\left[\dot{\hat{\epsilon}}_{kl} - \dot{\epsilon}_{kl}^{\varphi}([\![\dot{u}_i]\!], [\![\dot{u}_{i,j}]\!])\right] \tag{27}$$

where it was considered the arbitrariness of the function $\varphi(\mathbf{X})$ and the material character of $\mathcal{S}$, that is, once the orientation of the discontinuity surface is established, it becomes fixed throughout the analysis.

In addition, from the Eqs. (17) and (27) one can write:

$$\dot{\sigma}_{ij}^{\Omega\backslash\mathcal{S}} = E_{ijkl}^{o}\dot{\hat{u}}_{k,l} - E_{ijkl}^{o}\dot{\epsilon}_{kl}^{\varphi} \tag{28}$$

where the symmetries associated to the regime of small strains in isotropic media were taken into account.

Therefore, a first integral formulation of this problem can be obtained on the basis of the following equation of weighted residues, that is:

$$\begin{aligned}&\int_{\Omega\backslash\mathcal{S}}(\dot{\sigma}_{ij,j}^{\Omega\backslash\mathcal{S}} + \dot{b}_i)u_i^* d\Omega + \int_{\mathcal{S}} n_j(\dot{\sigma}_{ij}^{+} - \dot{\sigma}_{ij}^{-})u_i^* d\Gamma \\ &+ \int_{\Gamma_\sigma}(\dot{\bar{t}}_i - \dot{t}_i)u_i^* d\Gamma + \int_{\Gamma_u}(\dot{u}_i - \dot{\bar{u}}_i)t_i^* d\Gamma = 0\end{aligned} \tag{29}$$

where u_i^* and t_i^* represent weighted fields which, for the time being, are arbitrary.

In this way, based on the Eq. (29), and considering also the Eq. (28), we arrive at the integral governing equations of the boundary value problem, that is:

$$\begin{aligned}\dot{\hat{u}}_i(\boldsymbol{\xi}) &= \int_\Gamma u_{ij}^*(\boldsymbol{\xi},\mathbf{X})\dot{t}_j(\mathbf{X})d\Gamma(\mathbf{X}) - \int_\Gamma t_{ij}^*(\boldsymbol{\xi},\mathbf{X})\dot{\hat{u}}_j(\mathbf{X})d\Gamma(\mathbf{X}) \\ &+ \int_\Omega u_{ij}^*(\boldsymbol{\xi},\mathbf{X})\dot{b}_j(\mathbf{X})d\Omega(\mathbf{X}) + \int_\Omega \sigma_{ijk}^*(\boldsymbol{\xi},\mathbf{X})\dot{\epsilon}_{jk}^{\varphi}(\mathbf{X})d\Omega(\mathbf{X})\end{aligned} \tag{30}$$

$$\begin{aligned}c_{ij}(\boldsymbol{\xi})\dot{\hat{u}}_i(\boldsymbol{\xi}) &= \int_\Gamma u_{ij}^*(\boldsymbol{\xi},\mathbf{X})\dot{t}_j(\mathbf{X})d\Gamma(\mathbf{X}) - \int_\Gamma t_{ij}^*(\boldsymbol{\xi},\mathbf{X})\dot{\hat{u}}_j(\mathbf{X})d\Gamma(\mathbf{X}) \\ &+ \int_\Omega u_{ij}^*(\boldsymbol{\xi},\mathbf{X})\dot{b}_j(\mathbf{X})d\Omega(\mathbf{X}) + \int_\Omega \sigma_{ijk}^*(\boldsymbol{\xi},\mathbf{X})\dot{\epsilon}_{jk}^{\varphi}(\mathbf{X})d\Omega(\mathbf{X})\end{aligned} \tag{31}$$

$$\begin{aligned}\dot{\hat{\epsilon}}_{ij}(\boldsymbol{\xi}) &= \int_\Gamma u_{ijk}^*(\boldsymbol{\xi},\mathbf{X})\dot{t}_k(\mathbf{X})d\Gamma(\mathbf{X}) - \int_\Gamma t_{ijk}^*(\boldsymbol{\xi},\mathbf{X})\dot{\hat{u}}_k(\mathbf{X})d\Gamma(\mathbf{X}) \\ &+ \int_\Omega u_{ijk}^*(\boldsymbol{\xi},\mathbf{X})\dot{b}_k(\mathbf{X})d\Omega(\mathbf{X}) + \int_\Omega \sigma_{ijkl}^*(\boldsymbol{\xi},\mathbf{X})\dot{\epsilon}_{kl}^{\varphi}(\mathbf{X})d\Omega(\mathbf{X}) + F_{ijkl}^{\epsilon\epsilon}\dot{\epsilon}_{kl}^{\varphi}(\boldsymbol{\xi})\end{aligned} \tag{32}$$

In the Eqs. (30), (31) and (32) the tensors $u_{ij}^*(\boldsymbol{\xi},\mathbf{X})$, $t_{ij}^*(\boldsymbol{\xi},\mathbf{X})$ and $\sigma_{ijk}^*(\boldsymbol{\xi},\mathbf{X})$ are the fundamental Kelvin solutions and represent, respectively, displacements and surface forces in

the direction j and stress components jk, at a field point $\mathbf{X}$, due to a concentrated unit load at the source point $\boldsymbol{\xi}$ applied in the i direction. Already the tensors $u^*_{ijk}(\boldsymbol{\xi}, \mathbf{X})$, $t^*_{ijk}(\boldsymbol{\xi}, \mathbf{X})$ and $\sigma^*_{ijkl}(\boldsymbol{\xi}, \mathbf{X})$ represent the derivatives of Kelvin's fundamental solutions with respect to the source point $\boldsymbol{\xi}$ and the terms $F^{\epsilon\epsilon}_{ijkl}$ and $c_{ij}(\boldsymbol{\xi})$ are free terms associated with particular analytical integrations.

3.3 Equilibrium equation of the discontinuous interface

The integral equations presented in section 3.2 do not completely define the boundary value problem, since the internal continuity condition of the surface forces (Eq. (20)) is not met. Therefore, this condition is imposed separately, as in Oliver et al. (2003), adopting the strong form of the equation.

Initially we note that the Eq. (20) is equivalent to the following equation:

$$t_i(\mathbf{X}, t) = \sigma_{ij}^{\Omega\setminus\mathcal{S}}(\mathbf{X}, t)n_j(\mathbf{X}) = \sigma_{ij}^{\mathcal{S}}(\mathbf{X}, t)n_j(\mathbf{X}) \tag{33}$$

Therefore, considering the Eq. (33), together with the Eqs. (26) and (27), we obtain the interface equilibrium equation that is given by:

$$f_i = \left\{ E^o_{ijkl}\left[\hat{\epsilon}_{kl} - \epsilon^{\varphi}_{kl}([\![u_i]\!], [\![u_{i,j}]\!])\right] - \sigma^{\mathcal{S}}_{ij}(\epsilon_{ij}) \right\} = 0 \tag{34}$$

where ϵ_{ij} is given by the instant version of the Eq. (17) which, for points on $\mathcal{S}$, corresponds to the following expression:

$$\epsilon_{ij} = \hat{\epsilon}_{ij} - \epsilon^{\varphi}_{ij} + \frac{1}{2h}([\![u_i]\!]n_j + [\![u_j]\!]n_i) \tag{35}$$

In the context of the boundary element method the Eq. (34), called the equilibrium equation of the interface, can be solved numerically by the adoption of cells with embedded discontinuities that, in this case, provide the components of the displacements jump ($[\![u_i]\!]$) required to calculate ϵ^{φ}_{ij}. Furthermore, these components are considered to be constant within the cells causing null values for the gradient tensors, that is, $[\![u_{i,j}]\!] = 0$. In this way, considering a given regular strain $\hat{\epsilon}_{ij}$, and taking into account the Eq. (35), the Eq. (34) can be written as $f_i \equiv f_i([\![u_i]\!]) = 0$. Therefore, after the linearization of this equation its solution can be obtained through Newton's method.

From these considerations, a regularized constitutive equation that relates stresses and regular strains ($\hat{\epsilon}_{ij}$) is defined. Therefore, using the Eq. (27), we find:

$$\tilde{\sigma}_{ij}(\hat{\epsilon}_{ij}) = \sigma_{ij}^{\Omega\setminus\mathcal{S}}\left(\hat{\epsilon}_{ij} - \epsilon^{\varphi}_{ij}\left([\![u_i]\!](\hat{\epsilon}_{ij})\right)\right) = E^o_{ijkl}(\hat{\epsilon}_{kl} - \epsilon^{\varphi}_{kl}) \tag{36}$$

where $[\![u_i]\!](\hat{\epsilon}_{ij})$ represents the solution of Eq. (34).

4 IMPLICIT FORMULATION OF THE BOUNDARY ELEMENT METHOD FOR DISCONTINUITIES PROBLEMS

Equations (30), (31) and (32) can be rewritten in matrix form as:

$$\{\dot{u}^{\Omega}\} = [G^u]\{\dot{t}\} - [H^u]\{\dot{\hat{u}}\} + [Q^u_{\epsilon^{\varphi}}]\{\dot{\epsilon}^{\varphi}\} \tag{37}$$

$$[H]\{\dot{\hat{u}}\} = [G]\{\dot{t}\} + [Q_{\epsilon^{\varphi}}]\{\dot{\epsilon}^{\varphi}\} \tag{38}$$

$$\{\dot{\hat{\epsilon}}\} = [G^{\epsilon}]\{\dot{t}\} - [H^{\epsilon}]\{\dot{\hat{u}}\} + [Q^{\epsilon}_{\epsilon^{\varphi}}]\{\dot{\epsilon}^{\varphi}\} \tag{39}$$

From an algebraic manipulation of these equations we arrive at a single nonlinear equation, as well as in the implicit formulation developed by Telles and Carrer (1991). Therefore, through consideration of the essential and natural boundary conditions, the Eqs. (37), (38) and (39) are rewritten as:

$$\{\dot{\hat{u}}^{\Omega}\} = [A^u]\{\dot{x}\} + [B^u]\{\dot{y}\} + [Q^u_{\epsilon^\varphi}]\{\dot{\epsilon}^\varphi\} \tag{40}$$

$$[A]\{\dot{x}\} = [B]\{\dot{y}\} + [Q_{\epsilon^\varphi}]\{\dot{\epsilon}^\varphi\} \tag{41}$$

$$\{\dot{\hat{\epsilon}}\} = [A^\epsilon]\{\dot{x}\} + [B^\epsilon]\{\dot{y}\} + [Q^\epsilon_{\epsilon^\varphi}]\{\dot{\epsilon}^\varphi\} \tag{42}$$

where in $\{\dot{y}\}$ and $\{\dot{x}\}$ are grouped the prescribed and the unknown values of the boundary stemming from the vectors $\{\dot{\hat{u}}\}$ or $\{\dot{t}\}$. In addition, the matrices $[A]$ and $[B]$ are composed, respectively, by the coefficients from the matrices $[H]$ and $[G]$.

Isolating the vector $\{\dot{x}\}$ in the Eq. (41), we find:

$$\{\dot{x}\} = [N]\{\dot{y}\} + [M_{\epsilon^\varphi}]\{\dot{\epsilon}^\varphi\} \tag{43}$$

where we have that:

$$[N] = [A]^{-1}[B], \quad [M_{\epsilon^\varphi}] = [A]^{-1}[Q_{\epsilon^\varphi}] \tag{44}$$

Now replacing the Eq. (43) in the Eqs. (40) and (42), it is found:

$$\{\dot{\hat{u}}^{\Omega}\} = [N^u]\{\dot{y}\} + [M^u_{\epsilon^\varphi}]\{\dot{\epsilon}^\varphi\} \tag{45}$$

$$\{\dot{\hat{\epsilon}}\} = [N^\epsilon]\{\dot{y}\} + [M^\epsilon_{\epsilon^\varphi}]\{\dot{\epsilon}^\varphi\} \tag{46}$$

where:

$$[N^u] = [A^u][A]^{-1}[B] + [B^u], \quad [M^u_{\epsilon^\varphi}] = [A^u][A]^{-1}[Q_{\epsilon^\varphi}] + [Q^u_{\epsilon^\varphi}] \tag{47}$$

$$[N^\epsilon] = [A^\epsilon][A]^{-1}[B] + [B^\epsilon], \quad [M^\epsilon_{\epsilon^\varphi}] = [A^\epsilon][A]^{-1}[Q_{\epsilon^\varphi}] + [Q^\epsilon_{\epsilon^\varphi}] \tag{48}$$

The constitutive model considered in this work is independent of time, so the rates can be replaced by finite increments, that is, $\dot{(\cdot)} = \Delta(\cdot) \equiv (\cdot)_i - (\cdot)_{i-1}$, where the term i is an incremental indice. Thus, considering the i-th increment of prescribed loads $(\{y\})$, the Eqs. (43), (45) and (46) are rewritten as follows:

$$\{x\}^i = \lambda^i[N]\{y\} + [M_{\epsilon^\varphi}]\{\epsilon^\varphi\}^i \tag{49}$$

$$\{\hat{u}^{\Omega}\}^i = \lambda^i[N^u]\{y\} + [M^u_{\epsilon^\varphi}]\{\epsilon^\varphi\}^i \tag{50}$$

$$\{\hat{\epsilon}\}^i = \lambda^i[N^\epsilon]\{y\} + [M^\epsilon_{\epsilon^\varphi}]\{\epsilon^\varphi\}^i \tag{51}$$

where the term λ^i is a cumulative scalar value representing the load factor.

From the Eq. (51), and taking into account the matrix form of the regularized constitutive equation (Eq. (36)) applied to the complete set of internal cells, we define an equilibrium vector, $\{Q\}^i \equiv \{Q(\hat{\epsilon}^i, \lambda^i)\}$, as a function of the regular strains and the load factor, that is:

$$\{Q\}^i = \lambda^i[N^\epsilon]\{y\} + [M^\epsilon_{\epsilon^\varphi}]\big(\{\hat{\epsilon}\}^i - [E^o]^{-1}\{\tilde{\sigma}(\hat{\epsilon})\}^i\big) - \{\hat{\epsilon}\}^i = \{0\} \tag{52}$$

where $[E^o]$ now represents the linear elastic quasi-diagonal matrix and the vector $\{\tilde{\sigma}(\hat{\epsilon})\}$ represents the appropriate tensor vector.

It is observed that in Eq. (52) the initial strain fields do not appear explicitly. This fact justifies the implicit formulation nomenclature adopted by Telles and Carrer (1991).

5 SOLUTION STRATEGY

In this work the Eq. (52) is solved using the solution strategy implemented in INSANE software through the work of Peixoto et al. (2017). In this case, the load factor is considered an additional variable of $\{Q\}^i$. Therefore, we initially rewrite the Eq. (52) as:

$$\{Q\}^i = \lambda^i\{P\} - \{F\}^i = \{0\} \tag{53}$$

where:

$$\{P\} = [N^\epsilon]\{y\} \tag{54}$$

$$\{F\}^i = \{\hat{\epsilon}\}^i - [M^\epsilon_{\epsilon^\varphi}]\big(\{\hat{\epsilon}\}^i - [E^o]^{-1}\{\tilde{\sigma}(\hat{\epsilon})\}^i\big) \tag{55}$$

Linearizing the Eq. (53), we have that:

$$\{Q\}^i_{j-1} + \left[\frac{\partial\{Q\}}{\partial\{\hat{\epsilon}\}}\right]^i_{j-1}\{\delta\hat{\epsilon}\}^i_j + \left[\frac{\partial\{Q\}}{\partial\lambda}\right]^i_{j-1}\delta\lambda^i_j \approx \{0\} \tag{56}$$

where j is an iterative indice and $\delta(\cdot)^i_j = (\cdot)^i_j - (\cdot)^i_{j-1}$. In this way, we find:

$$[D]^i_{j-1}\{\delta\hat{\epsilon}\}^i_j = \delta\lambda^i_j\{P\} + \{Q\}^i_{j-1} \tag{57}$$

where $[D]^i_{j-1}$ is given by:

$$[D]^i_{j-1} = \left[[I] - [M^\epsilon_{\epsilon^\varphi}][E^o]^{-1}\left([E^o] - \left[\frac{\partial\tilde{\sigma}}{\partial\hat{\epsilon}}\right]^i_{j-1}\right)\right] \tag{58}$$

In the Eq. (58) the term $[I]$ is an identity matrix and $\left[\frac{\partial\tilde{\sigma}}{\partial\hat{\epsilon}}\right]$ is assembled, for cells in linear regime, from the elastic constitutive tensor E^o_{ijkl} (Eq. (8)) and for cells in strong discontinuity regime, from the following equation (Peixoto et al., 2017):

$$\left[\frac{\partial\tilde{\sigma}}{\partial\hat{\epsilon}^c}\right] = [E^o]\left([I] - [\nabla^s\varphi]\left[\frac{\partial\{f\}}{\partial\{[\![u^c]\!]\}}\right]^{-1}[\bar{N}^c]^T\left([E^o] - \left[\frac{\partial\sigma^{\mathcal{S}}}{\partial\epsilon}\right]\right)\right) \tag{59}$$

where the terms $(\cdot)^c$ are referring to cells with embedded discontinuity and the term ∇^s refers to the gradient of the symmetric part. In addition, the matrix $[\bar{N}^c]$ is composed by the components of the unit vector n_i, that is:

$$[\bar{N}^c] = \begin{bmatrix} n_1 & 0 \\ 0 & n_2 \\ n_2 & n_1 \end{bmatrix} \tag{60}$$

Now decomposing the iterative correction vector of the regular strains $(\{\delta\hat{\epsilon}\}^i_j)$, present in the Eq. (57), it is found:

$$\{\delta\hat{\epsilon}\}^i_j = \delta\lambda^i_j\{\hat{\epsilon}^P\}^i_j + \{\delta\hat{\epsilon}^Q\}^i_j \tag{61}$$

where the terms $\{\hat{\epsilon}^P\}_j^i$ and $\{\delta\hat{\epsilon}^Q\}_j^i$ satisfy the following equations, respectively:

$$[D]_{j-1}^i\{\hat{\epsilon}^P\}_j^i = \{P\} \tag{62}$$
$$[D]_{j-1}^i\{\delta\hat{\epsilon}^Q\}_j^i = \{Q\}_{j-1}^i \tag{63}$$

That is, $\{\hat{\epsilon}^P\}_j^i$ corresponds to the solution due to the external load $\{P\}$ and $\{\delta\hat{\epsilon}^Q\}_j^i$ is associated with the residue of the global equilibrium condition $(\{Q\}_{j-1}^i)$.

Decomposing also the expressions for the iterative corrections that contains the boundary unknowns $(\{\delta x\}_j^i)$ and the internal displacements $(\{\delta\hat{u}^\Omega\}_j^i)$, we have:

$$\{\delta x\}_j^i = \{x\}_j^i - \{x\}_{j-1}^i = \delta\lambda_j^i[N]\{y\} + [M_{\epsilon^\varphi}]\{\delta\epsilon^\varphi\}_j^i \tag{64}$$
$$\{\delta\hat{\epsilon}\}_j^i = \{\hat{\epsilon}\}_j^i - \{\hat{\epsilon}\}_{j-1}^i = \delta\lambda_j^i[N^\epsilon]\{y\} + [M_{\epsilon^\varphi}^\epsilon]\{\delta\epsilon^\varphi\}_j^i \tag{65}$$

where the Eqs. (49) and (51) were considered.

Isolating in the Eq. (65) the vector $\{\delta\epsilon^\varphi\}_j^i$ and replacing the result in the Eq. (64), we find:

$$\{\delta x\}_j^i = \delta\lambda_j^i\{x^P\}_j^i + \{\delta x^Q\}_j^i \tag{66}$$

where the Eqs. (54), (61) and (62) were considered. In addition, in the Eq. (66) the following relations are valid:

$$\{x^P\}_j^i = [N]\{y\} + [M_{\epsilon^\varphi}][M_{\epsilon^\varphi}^\epsilon]^{-1}\big([I] - [D]_{j-1}^i\big)\{\hat{\epsilon}^P\}_j^i \tag{67}$$
$$\{\delta x^Q\}_j^i = [M_{\epsilon^\varphi}][M_{\epsilon^\varphi}^\epsilon]^{-1}\{\delta\hat{\epsilon}^Q\}_j^i \tag{68}$$

Now starting from the Eq. (50), we find the following expression for $\{\delta\hat{u}^\Omega\}_j^i$, that is:

$$\{\delta\hat{u}^\Omega\}_j^i = \delta\lambda_j^i\{\hat{u}^{\Omega,P}\}_j^i + \{\delta\hat{u}^{\Omega,Q}\}_j^i \tag{69}$$

where:

$$\{\hat{u}^{\Omega,P}\}_j^i = [N^u]\{y\} + [M_{\epsilon^\varphi}^u][M_{\epsilon^\varphi}^\epsilon]^{-1}\big([I] - [D]_{j-1}^i\big)\{\hat{\epsilon}^P\}_j^i \tag{70}$$
$$\{\delta\hat{u}^{\Omega,Q}\}_j^i = [M_{\epsilon^\varphi}^u][M_{\epsilon^\varphi}^\epsilon]^{-1}\{\delta\hat{\epsilon}^Q\}_j^i \tag{71}$$

The solution strategy algorithm is synthesized through the following table.

SOLUTION STRATEGY ALGORITHM

i. Calculate: $\{P\}$, using the Eq. (54) and initialize $i = 0$;

ii. $i = i + 1$, $j = 0$;

iii. If $i >$ maximum number of increments specified $\Rightarrow$ END;

iv. $\{Q\}_j^i = \{0\}$, $\{F\}_j^i = \{0\}$;

v. $j = j + 1$;

vi. If $j >$ maximum number of iterations specified, processing is interrupted;

vii. The matrix $[D]_{j-1}^i$ of the Eq. (58) is assembled;

viii. The Eqs. (62) and (63) are solved for $\{\hat{\epsilon}^P\}_j^i$ and $\{\delta\hat{\epsilon}^Q\}_j^i$;

ix. $\{x^P\}_j^i$, $\{\delta x^Q\}_j^i$, $\{\hat{u}^{\Omega,P}\}_j^i$ and $\{\delta\hat{u}^{\Omega,Q}\}_j^i$ are calculated using the Eqs. (67), (68), (70) and (71);

x. $\delta\lambda_j^i$ is calculated using a control method;

xi. $\{\delta\hat{\epsilon}\}_j^i$, $\{\delta x\}_j^i$ and $\{\delta\hat{u}^{\Omega}\}_j^i$ are assembled from the Eqs. (61), (66) and (69);

xii. λ_j^i, $\{\hat{\epsilon}\}_j^i$, $\{x\}_j^i$ and $\{\hat{u}^{\Omega}\}_j^i$ are updated by doing $(\cdot)_j^i = (\cdot)_{j-1}^i + \delta(\cdot)_j^i$;

xiii. $\{F\}_j^i$ is assembled using the Eq. (55);

xiv. $\{Q\}_j^i = \lambda_j^i\{P\} - \{F\}_j^i$ is calculated (Eq. (53));

xv. Convergence test:
If $\dfrac{\parallel \{Q\}_j^i \parallel}{\parallel \lambda_j^i\{P\} \parallel} <$ TOL, returns to step (ii) for the next load increment, otherwise, returns to step (v) for new iteration.

6 NUMERICAL EXAMPLE

In this section, the implicit formulation of the boundary element method is used, with the solution strategy presented in section 5, for the mixed-mode fracture simulation of a pre-notched concrete beam subjected to shear with forces at four points. In this analysis, the isotropic damage model presented in the section 2.1 together with the exponential softening law outlined in the section 2.2 are take into account.

A schematic model of this test, which has been studied experimentally by Arrea and Ingraffea (1982), is presented in the Fig. 2 where it shows the geometric properties, loads, boundary conditions and the approximate trajectory of the crack obtained in the experiments. In addition, the values considered in the numerical analyzes for the elasticity modulus E, Poisson's ratio ν, tensile strength f_t and fracture energy G_f are also presented.

The simulations were performed using only cells with constant jumps for the displacement components and 642 linear elements were considered in the discretization of the boundary. Thus, a square cell with a diagonal of 1.6 mm was pre-introduced at the notch tip. In this case, the origin of the discontinuity segment within the cell is established as the midpoint of the side common to the boundary of the notch.

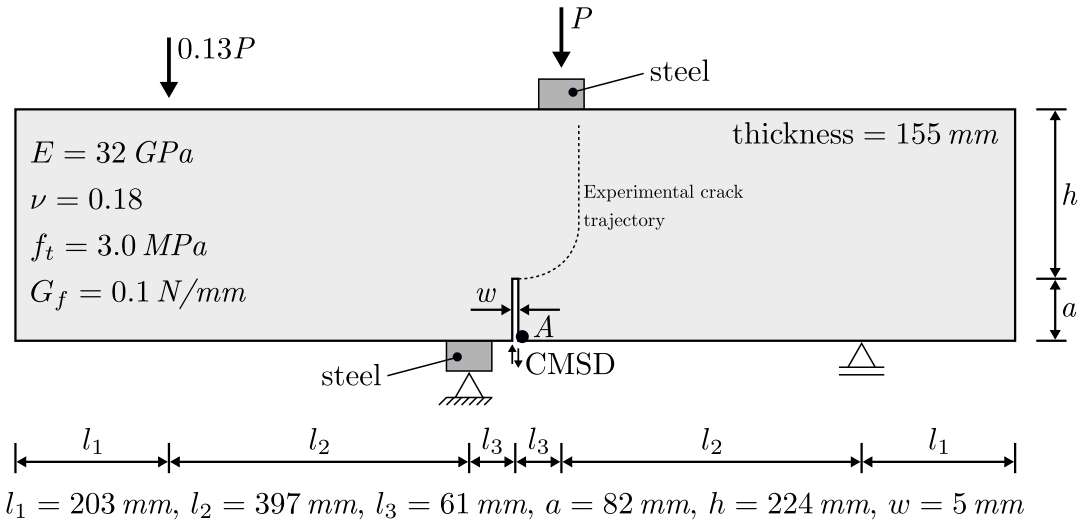

Figure 2: Shear test with forces at four points

In the nonlinear analysis the vertical displacement component of point A (Fig. 2) was controlled and a convergence tolerance equal to TOL $= 1 \times 10^{-4}$ was adopted in the incremental-iterative process. In addition, we considered the plane stress state and the direct introduction of strong discontinuity at the end of the elastic regime with $k = 0.01$ mm (Eqs. (14) and (15)).

Analyzes were performed with cell generation only at the end of the step convergence and at any iteration considering, for each of these cases, simulations with 40, 70 and 170 steps. Thus, the results for the applied load versus the relative vertical displacement between the two sides at the initial tip of the notch (*crack mouth sliding displacement* - CMSD) are presented through the Figs. 3 and 4. In these figures the experimental envelope obtained by Arrea and Ingraffea (1982) is also outlined.

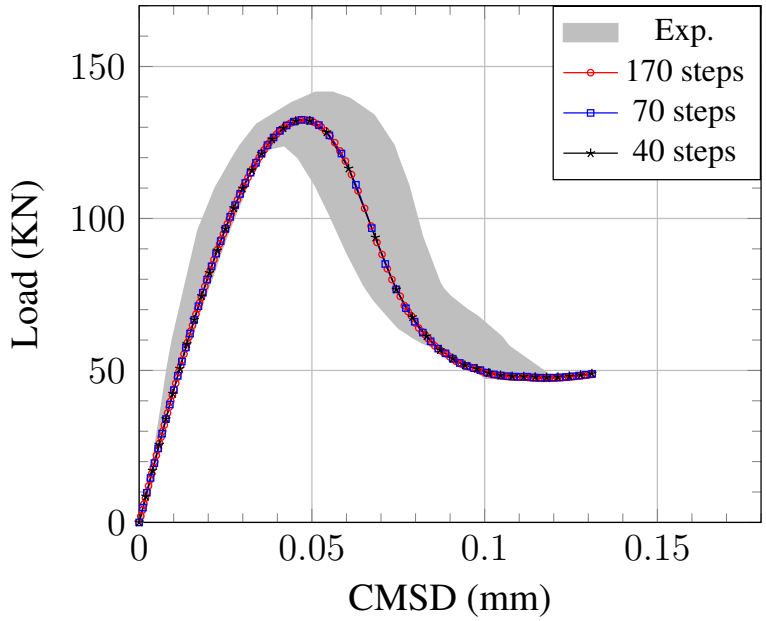

Figure 3: Results for load *P* versus CMSD (*Crack Mouth Sliding Displacement*) with cell generation at any iteration

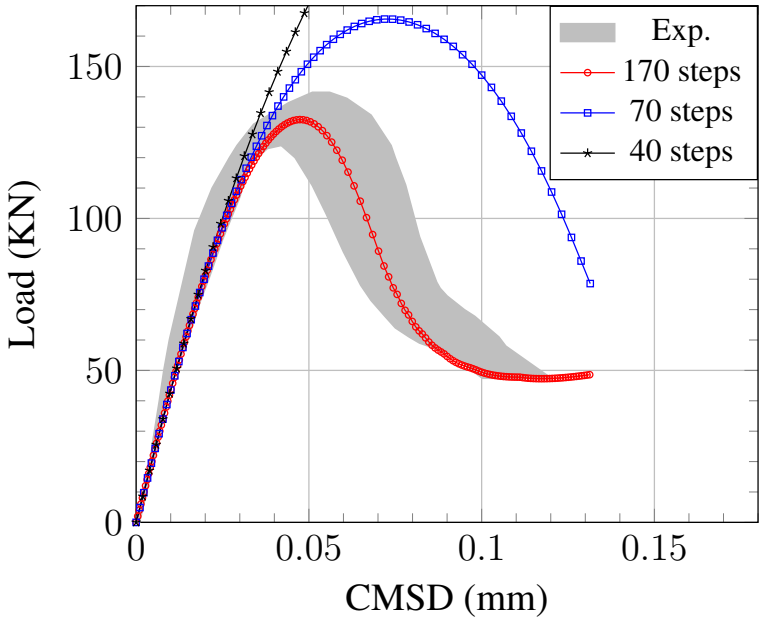

Figure 4: Results for load *P* versus CMSD (*Crack Mouth Sliding Displacement*) with cell generation only after step convergence

As can be seen from the Fig. 3 the curves obtained for all the 3 simulations were practically coincident and also had a very satisfactory approximation with the experimental results. However, the same is not observed for the curves obtained considering cell generation after step convergence (Fig. 4). In this case, the three curves presented very different profiles and, in addition, only the curve obtained in the simulation with 170 steps presented satisfactory agreement with the experimental results.

In the latter case, the number of cells with embedded discontinuity generated is proportional to the number of steps used in the analysis. Thus, the smaller the number of steps the more rigid the model will be, which explains, therefore, the different profiles sketched through the Fig. 4. As can be seen from this figure, the curve in the analysis with 40 steps has the profile quite close to that of a straight line and already for the curve obtained using 70 steps a slight softening was observed with a peak still much higher than those presented by the experimental results. Finally, for the results obtained using 170 steps, it is observed that the curve was almost all inserted in the experimental envelope and, in addition, the profile of this curve was very close to those presented through the Fig. 3.

7 CONCLUSION

In this work, the mixed-mode fracture simulation of a pre-notched concrete beam subjected to shear with forces at four points was performed. In this way the implicit formulation of the boundary element method was used considering three different step sizes in the incremental-iterative process of the nonlinear analysis. Therefore, it was found that the curves obtained for the applied load versus the CMSD presented different aspects when the cells with embedded discontinuity were generated at any iteration and only after the step convergence.

In the first analyzes, where the generation of cells was considered at any iteration, step size independence was observed in the structural response, since all the three curves obtained

presented practically identical profiles. In addition, the results showed good accuracy with the experimental results even with the generation of cells occurring in an unbalanced state. For cells generated after step convergence, that is the most correct form from the numerical point of view, a strong dependence on the step size was observed verified through the three different profiles found for these curves. In this case, we verified that the number of steps is proportional to the number of cells generated which, in turn, are directly related to the softening or hardening of the model.

It is important to note that only monotonic loads were considered in the numerical analyzes, therefore, for other types of loads the conclusions obtained in this work may not be valid.

ACKNOWLEDGEMENTS

The authors would like to acknowledge CNPq (National Council of Scientific and Technological Development), CAPES (Coordination of Improvement of Higher Education Personnel), FAPEMIG (Minas Gerais State Research Foundation) and PROPEEs/UFMG (Structure Engineering Graduate Program of the Federal University of Minas Gerais) for financial supports.

REFERENCES

Arrea, M. and Ingraffea, A. R. (1982). Mixed-mode crack propagation in mortar and concrete. Technical report, 81-13, Department of Structural Engineering, Cornell University, Ithaca, USA.

Manzoli, O., Oliver, J., and Cervera, M. (1998). Localización de deformación: Análisis y simulación numérica de discontinuidades en mecánica de sólidos. Centro Internacional de Métodos Numéricos en Ingeniería (CIMNE). Monografía n. 44. Barcelona.

Manzoli, O. L., Pedrini, R. A., and Venturini, W. S. (2009). Strong discontinuity analysis in solid mechanics using boundary element method. In Spountzakis, E. J. and Aliabadi, M. H., editors, *Avances in Boundary Element Techniques X*, pages 323–329, Atenas, Grécia.

Manzoli, O. L. and Venturini, W. S. (2004). Uma formulação do MEC para simulação numérica de descontinuidades fortes. *Revista Internacional de Métodos Numéricos para Cálculo y Diseño en Ingeniería*, 20(3):215–234.

Manzoli, O. L. and Venturini, W. S. (2007). An implicit BEM formulation to model strong discontinuities. *Computational Mechanics*, 40:901–909.

Oliver, J. (1996a). Modelling strong discontinuities in solid mechanics via strain softening constitutive equations. Part 1: Fundamentals. *International Journal for Numerical Methods in Engineering*, 39:3575–3600.

Oliver, J. (1996b). Modelling strong discontinuities in solid mechanics via strain softening constitutive equations. Part 2: Numerical simulation. *International Journal for Numerical Methods in Engineering*, 39:3601–3623.

Oliver, J. (2000). On the discrete constitutive models induced by strong discontinuity kinematics and continuum constitutive equations. *International Journal of Solids and Structures*, 37:7207–7229.

Oliver, J., Cervera, M., and Manzoli, O. (1998). On the use of strain-softening models for the simulation of strong discontinuities in solids. In de Borst, R. and van der Giessen, E., editors, *Material instabilities in solids*, chapter 8, pages 107–123. John Wiley & Sons, Chichester.

Oliver, J., Cervera, M., and Manzoli, O. (1999). Strong discontinuities and continuum plasticity models: the strong discontinuity approach. *International Journal of Plasticity*, 15:319–351.

Oliver, J., Huespe, A. E., Blanco, S., and Linero, D. L. (2006). Stability and robustness issues in numerical modeling of material failure with the strong discontinuity approach. *Computer Methods in Applied Mechanics and Engineering*, 195:7093–7114.

Oliver, J., Huespe, A. E., Pulido, M. D. G., and Chaves, E. (2002). From continuum mechanics to fracture mechanics: the strong discontinuity approach. *Engineering Fracture Mechanics*, 69:113–136.

Oliver, J., Huespe, A. E., and Samaniego, E. (2003). A study on finite elements for capturing strong discontinuities. *International Journal for Numerical Methods in Engineering*, 56:2135–2161.

Pedrini, R. A. A. (2008). Análise de propagação arbitrária de descontinuidades fortes em sólidos bidimensionais pelo método dos elementos de contorno. Master's thesis, Universidade de São Paulo, São Carlos.

Peixoto, R. G., Ribeiro, G. O., and Pitangueira, R. L. S. (2016). Concrete fracture analysis using the continuum strong discontinuity approach and the boundary element method. In Ávila, S. M., editor, *Proceedings of the XXXVII Iberian Latin-American Congress on Computational Methods in Engineering - CILAMCE*, Brasília, DF, Brasil.

Peixoto, R. G., Ribeiro, G. O., Pitangueira, R. L. S., and Penna, S. S. (2017). The strong discontinuity approach as a limit case of strain localization in the implicit BEM formulation. *Engineering Analysis with Boundary Elements*, 80:127–141.

Simo, J. C., Oliver, J., and Armero, F. (1993). An analysis of strong discontinuities induced by strain-softening in rate-independent inelastic solids. *Computational Mechanics*, 12:277–296.

Telles, J. C. F. and Carrer, J. A. M. (1991). Implicit procedures for the solution of elastoplastic problems by the boundary element method. *Mathematical and Computer Modelling*, 15:303–311.